Multi-View Slot Attention Using Paraphrased Texts for Face Anti-Spoofing

Jeongmin Yu[1*], Susang Kim[1,2*], Kisu Lee[1], Taekyoung Kwon[1], Won-Yong Shin[1], Ha Young Kim[1†]
[1]Yonsei University [2]POSCO DX
{jeongminyu, healess, kisu0928, taekyoung, wy.shin, hayoung.kim}@yonsei.ac.kr

Abstract

*Recent face anti-spoofing (FAS) methods have shown remarkable cross-domain performance by employing vision-language models like CLIP. However, existing CLIP-based FAS models do not fully exploit CLIP's patch embedding tokens, failing to detect critical spoofing clues. Moreover, these models rely on a single text prompt per class (*e.g.*, 'live' or 'fake'), which limits generalization. To address these issues, we propose MVP-FAS, a novel framework incorporating two key modules: Multi-View Slot attention (MVS) and Multi-Text Patch Alignment (MTPA). Both modules utilize multiple paraphrased texts to generate generalized features and reduce dependence on domain-specific text. MVS extracts local detailed spatial features and global context from patch embeddings by leveraging diverse texts with multiple perspectives. MTPA aligns patches with multiple text representations to improve semantic robustness. Extensive experiments demonstrate that MVP-FAS achieves superior generalization performance, outperforming previous state-of-the-art methods on cross-domain datasets. Code: https://github.com/Elune001/MVP-FAS.*

1. Introduction

Face anti-spoofing (FAS), which distinguishes spoofed faces from real ones, has become essential for enhancing the security of facial recognition systems. Previous FAS models [3, 4, 11, 26, 29, 30, 44, 61] have demonstrated notable effectiveness against various attack types, such as printed image [65], replay [9], and 3D mask attacks [17] in intra-domain datasets. However, in real-world scenarios, FAS models may encounter unseen attack types and data not present during training [24, 47, 54]. Therefore, extracting generalized features is crucial to enhancing FAS models' ability to accurately detect spoofed faces across a broader range of conditions [19, 22, 27, 32, 36, 68].

Recently, FAS methods [7, 14, 18, 20, 31, 36, 39, 49] that leverage vision-language models (VLMs), such as

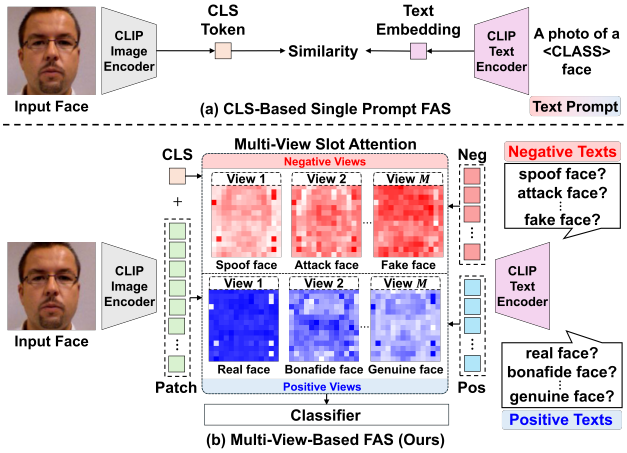

Figure 1. **Comparison between CLS-based single prompt and multi-view-based FAS methods.** (a) illustrates the single prompt FAS model using the CLIP CLS token, which captures global information but lacks fine-grained local details. (b) represents our multi-view-based FAS framework (MVP-FAS), providing local details with global context for each view. The red and blue areas indicate where the model focuses on within each view.

CLIP [45], have demonstrated remarkable performance in zero-shot learning and domain generalization across diverse cross-domain attacks. The first CLIP-based FAS model, FLIP [49], primarily relies on the classification token (CLS token), which encodes global image information. Recent CLIP-based models [18, 20, 36] have proposed methods to utilize local spoofing clues. FGPL [20] captures local details through prompt learning and a convolutional adapter applied to the CLIP image encoder. CFPL [36] and S-CPTL [18] leverage spatial information by extracting style- or content-related features from patch embeddings and feeding them into the text encoder. However, these methods [18, 20, 36] still do not directly utilize CLIP's patch embedding tokens, which contain rich local information within the image domain. Consequently, similar to FLIP [49], these approaches struggle to capture fine-grained spoofing artifacts, such as abnormal textures and light reflections in small areas, due to the information loss when projecting into the text embedding space for prompt generation. In addition, CLIP is trained to align the CLS token

*Equal contribution
†Corresponding author

with the text embedding without applying direct supervision to the patch embeddings during training. Thus, explicitly aligning local patch embeddings with text embeddings is necessary for effectively leveraging fine-grained local information.

Furthermore, as shown in previous studies [18, 20, 36, 39], the input text prompt is another important factor in CLIP-based FAS. These works have explored prompt learning methods that integrate image features, enhancing text descriptions beyond fixed prompts. However, they still use only a single fixed text pair to represent the real and spoof classes, such as 'live' and 'fake'. Since vanilla CLIP is not specifically trained for the FAS task, there is no guarantee that the class texts used to represent 'spoof' or 'real' have semantics that are generally applicable in FAS. For instance, the word 'live' can indicate a real face in FAS but can also mean live stream. Therefore, as shown in prior research [49] and our observation (see Sec. 4.3.2), relying on a single fixed text prompt per class can limit the model's robustness, affecting generalization performance.

To address these challenges, we propose a novel framework, **M**ulti-**V**iew cli**P** for **FAS** (**MVP-FAS**), which comprises two main modules: Multi-View Slot attention (**MVS**) and Multi-Text Patch Alignment (**MTPA**). Both modules leverage various paraphrases of the class text to enhance generalization. MVS extracts multi-view representations that capture local spoofing details and global context based on slot attention, where global-aware CLIP patch embeddings serve as queries and paraphrased text embeddings as keys and values. As shown in Fig. 1 (b), MVS enables the model to interpret patches from various perspectives of multiple texts, leading to more generalized features. MTPA aligns patch embeddings with a multi-text anchor derived from paraphrased texts, which improves alignment robustness by alleviating the impact of biased text representations in the embedding space. By incorporating soft-masking, MTPA effectively aligns patches that are relatively important for spoofing prediction.

We evaluate MVP-FAS through extensive experiments on two protocols: Protocol 1 [5, 9, 57, 65] and Protocol 2 [16, 34, 64], both designed for cross-domain datasets. MVP-FAS achieves state-of-the-art (SOTA) cross-domain generalization performance by a large margin on both protocols in FAS. Notably, TPR@FPR=1% is consistently high overall, demonstrating its reliability in high-security scenarios. Furthermore, our method visualizes attention scores for each class, supporting better decision-making and highlighting its potential for enhanced interpretability. To summarize, our main contributions are as follows:

- We introduce MVS to extract generalized multi-view features by using multi-text with slot attention, enabling them to capture detailed local and global information from patch embeddings across diverse perspectives.
- We design MTPA, which aligns CLIP's patch embeddings with multiple paraphrased texts using soft-masking, improving semantic robustness and alignment effectiveness.
- Our model achieves SOTA performance across various cross-domain FAS datasets, demonstrating that integrating MVS and MTPA enhances generalization.
- We visualize the multi-view attention weights from MVS, offering more informative, region-based insights about the predictions than existing visualization methods.

2. Related Work

Face Anti-Spoofing. FAS has been studied for over a decade driven by increasingly sophisticated spoofing techniques. Early methods [3, 4, 11, 26, 44, 61] relied on handcrafted features to identify counterfeits [30, 43]. With advances in deep learning, FAS has evolved into an end-to-end learning using convolutional neural networks for feature extraction and classification [29, 63]. However, these approaches often struggle with cross-domain generalization. To address this, domain adaptation techniques [28, 40] attempt to minimize distributional differences between the source and target domains, though their effectiveness depends on the availability of unlabeled target data. An alternative is domain generalization [27, 37, 38, 50, 56, 67], which leverages multiple source domains without requiring target data. However, most existing methods rely on labeled images, limiting their ability to generalize across diverse real-world conditions.

CLIP-based FAS. CLIP [45] has driven significant progress in VLMs, inspiring advancements across various domains such as visual question answering [51], semantic segmentation [42, 69], and domain generalization [52]. In FAS, various CLIP-based models [18, 20, 36, 39, 49] have been proposed with prompt learning, employing CLIP's zero-shot transfer learning capabilities. FLIP [49] is the first to utilize heuristic positive and negative prompt pairs for fine-tuning CLIP models, aligning real and fake images with corresponding prompts to enhance overall FAS performance. CFPL [36] introduces class-free prompt learning, emphasizing content and style of the face. FGPL [20] employs domain-agnostic information through prompt learning, while S-CPTL [18] reflects visual style information via prompt learning. BUDoPT [39] addresses varying domain prompt levels, including recording settings and attack types. However, these methods rely on CLIP's patch embeddings within the prompt learning framework, potentially causing information loss compared to direct utilization. Consequently, they may struggle to effectively capture local spoofing clues in the image domain.

Object-Centric Learning. Object-centric learning has received substantial interest for its ability to generate semantically disentangled representations. The slot attention mechanism [41] groups the features with similar characteristics

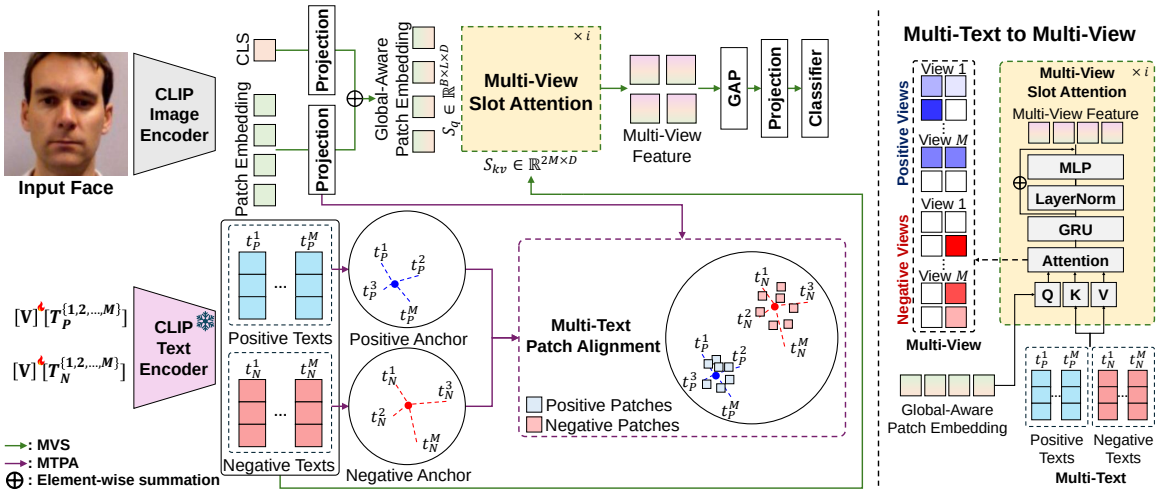

Figure 2. **The overall architecture of MVP-FAS.** t indicates the text embedding of the input prompt after passing through the text encoder.

around a slot query in an object-centric manner, allowing each slot to represent a distinct object part. Several studies [13, 23, 46, 58–60] have employed image tokens within the slot attention to cluster similar features effectively. Slot-VLM [59] effectively bridges the gap between vision and language by leveraging object-centric and event-centric slots. GeoVLN [23] extends slot-based visual representation learning to enhance robust navigation, while the binding module [58] uses slot attention to cluster image tokens into groups. Inspired by these approaches, we first introduce a variant of slot attention with a multi-text approach to enhance generalization in FAS.

Patch-Level Alignment in CLIP. In CLIP, the visual encoder's CLS token and the text encoder's features are well aligned for image-text pairs. However, CLIP mainly learns global information [45] during training, making it struggle to encode fine-grained details in patch embeddings. Recent studies propose methods for aligning CLIP's patch embeddings with text to enhance detailed information [2, 35, 42]. PACL [42] introduces a modified CLIP's contrastive loss to enhance the alignment between visual patch embeddings and text encoder features, while FM-CLIP [35] attempts to guide patch-level representations by adding text features into the patches, weighted according to their similarity. Ke Fan *et al.* [13] also show that fine-tuning CLIP with cross-attention using CLS token and patch embeddings enhances object localization. While previous studies focused on single patch-text alignment, aligning multiple semantically equivalent texts with patches has been unexplored, despite its potential to enhance robustness.

3. Method

3.1. Overall Architecture

The architecture of MVP-FAS is shown in Fig. 2. MVP-FAS leverages the CLIP image encoder $\mathcal{V}(\cdot)$ and text encoder $\mathcal{T}(\cdot)$, where the text encoder is frozen to retain pre-trained linguistic knowledge, while the image encoder is fine-tuned to adapt to the FAS task.

Text Encoder. To obtain multi-view features, we utilize positive texts $T_P = \{T_P^j\}_{j=1}^M$ for real faces and negative texts $T_N = \{T_N^j\}_{j=1}^M$ for spoof faces, where M is the number of views. All positive and negative texts are generated using ChatGPT [1] as paraphrases of the texts 'real face' and 'spoof face'. The input prompt $\mathcal{P}$ for the text encoder consists of a class text [CLASS] $\in T_P \cup T_N$ and context texts $[\mathbf{V}]$, as shown in Eq. (1). Specifically, we employ the learnable prompt of CoOp [66] for the context texts to find more suitable text representations for FAS.

$$\mathcal{P} = [\mathbf{V}][\text{CLASS}]. \tag{1}$$

As a result, the set of input prompts are fed into the text encoder, resulting in the output multi-text embeddings $S_{kv} \in \mathbb{R}^{2M \times D}$, where D denotes the embedding dimension.

Image Encoder. Image encoder receives a batch of face images $I \in \mathbb{R}^{B \times H \times W \times 3}$ as input and extracts a CLS token and patch embeddings, where B is the batch size and H, W are the image resolutions. They are each passed through separate projection layers, each consisting of two-layer multilayer perceptron (MLP) to adjust dimensions to D. Subsequently, the CLS token is broadcast across all patch embeddings, creating global-aware patch embeddings $S_q \in \mathbb{R}^{B \times L \times D}$, where L denotes the patch embedding length.

Feature Extraction and Classification. Finally, MVP-FAS leverages MVS to transform the global-aware patch embedding into generalized multi-view features, integrating global context and local detailed information based on multi-text embeddings from the text encoder. The resulting multi-view features are then fed into a classification head, which comprises global average pooling, a two-layer MLP

Algorithm 1 Multi-View Slot Attention Module.

Input: $S_q \in \mathbb{R}^{B\times L\times D}$, $S_{kv} \in \mathbb{R}^{2M\times D}$
$S_{kv} = \text{repeat}(S_{kv}, \text{dim=0}, \text{repeats=}B) \in \mathbb{R}^{B\times 2M\times D}$
$S_{kv} = \text{LayerNorm}(S_{kv})$
$k, v = \text{Linear}_k(S_{kv}), \text{Linear}_v(S_{kv})$
for $i = 1$ to i_{max} **do**
  $S_{q_{\text{prev}}} = S_q$
  $q = \text{Linear}_q(\text{LayerNorm}(S_q))$
  $attn = \text{softmax}(q \cdot k^T \frac{1}{\sqrt{D}}, \text{axis='query'})$
  # Multi-Text to Multi-View
  $attn = attn/(\sum(attn, \text{axis='key'}) + \epsilon)$
  $updates_{MV} = attn \cdot v$ # Aggregate Views
  $S_q = \text{GRU}(updates_{MV}, S_{q_{\text{prev}}})$ # Feature Update
  $S_q = S_q + \text{MLP}(\text{LayerNorm}(S_q))$
$\text{F}_{MV} = S_q$
return F_{MV} ▷ Return Multi-View Feature

as a projection layer, and a fully connected layer as a classifier to predict whether the face is real or spoofed.

3.2. Multi-View Slot Attention for VLMs

Previous works [18, 36] project image-level detailed information into the text embedding space via prompts, which can lead to the loss of visual characteristics. To address this problem, MVS directly utilizes CLIP's patch embeddings based on slot attention [41] to preserve the fine-grained details of local patches.

Unlike conventional slot attention, our MVS uses global-aware patch embeddings as queries and text embeddings as keys and values. This design enables the global assignment of text embeddings while preserving the details of local patches, preventing information loss when patches are assigned to learnable queries in the standard slot attention. As described in Algorithm 1, to allocate text embedding to each global-aware patch embedding, MVS projects global-aware patch embeddings into patch queries $q \in \mathbb{R}^{B\times L\times D}$ and text embeddings into text keys $k \in \mathbb{R}^{B\times 2M\times D}$ and values $v \in \mathbb{R}^{B\times 2M\times D}$. Then, MVS calculates the similarity between queries and keys through a scaled dot product and applies softmax along the query dimension L to compute the attention scores $attn_{(q,k)} \in \mathbb{R}^{B\times L\times 2M}$.

$$attn_{(q,k)} = \text{softmax}(q \cdot k^{\text{T}} \frac{1}{\sqrt{D}}, \text{axis='query'}). \quad (2)$$

These attention scores are used to assign positive and negative class texts to the patches.

Single-view ($M = 1$). Guided by attention scores, a single pair of positive and negative text values is allocated across all patch queries. As shown in Fig. 3 (a), global-aware patches S_q are updated with the update value ΔS_q, which is separated text values $attn_{(q,k)}v$ and serves as input to the

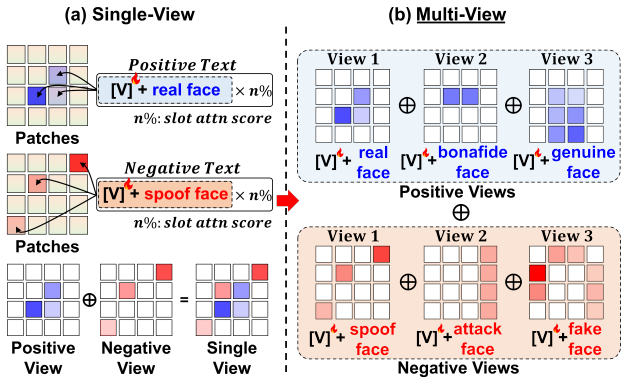

Figure 3. **The mechanism for binding text embeddings to patch embeddings in Multi-View Slot attention (MVS).** (a) depicts a single-view setting with $M = 1$, while (b) illustrates a multi-view example where $M = 3$. Each text embedding is distributed across patches based on the slot attention score of $n\%$. All positive-negative view pairs are aggregated via element-wise summation ($\oplus$), resulting in the final multi-view output.

GRU [10], while S_q is used as its hidden state.

$$S_q{}' = \text{GRU}(\Delta S_q, S_q), \quad \text{where } \Delta S_q = attn_{(q,k)}v. \quad (3)$$

Specifically, the updated patches $S_q{}'$ are refined through the residual MLP in Algorithm 1, expressed as follows:

$$S_q{}' \leftarrow S_q{}' + \text{MLP}(\text{LayerNorm}(S_q{}')). \quad (4)$$

This slot attention process preserves local patch information, which is crucial for spoofing prediction, employing a GRU when updating additional text values. By leveraging the semantics of distributed text values, the model effectively captures the global context among local patches while preserving essential patch information. Concretely, as shown at the bottom of Fig. 3 (a), the positive and negative views derived from a single text pair are combined to form a single-view representation, which considers an image from both perspectives.

$$\Delta S_q = attn_{(q,k_p)}v_p + attn_{(q,k_n)}v_n, \quad (5)$$

where (k_p, k_n) and (v_p, v_n) are keys and their corresponding values of positive-negative text embeddings, respectively. Through this process, the model focuses on semantically meaningful regions in the single-view representation. However, a limitation of single-view slot attention is that the model's performance depends on the choice of prompt.

Multi-view ($M > 1$). To improve generalization, MVS leverages paraphrased texts with the same meaning, similar to rephrasing search keywords to retrieve more useful information online. As illustrated in Fig. 3 (b), MVS takes multiple positive and negative text pairs as input and generates various positive and negative views corresponding to multi-text pairs. By combining these views, MVS generates

multi-view representations that enable the model to capture more generalized and robust features.

Specifically, the update value of global-aware patch embeddings ΔS_q can be represented as a weighted summation based on attention scores corresponding to the positive and negative text values $v \in \mathbb{R}^{B\times 2M\times D}$.

$$\Delta S_q = \sum_{j=1}^{2M} attn_{(q,k_j)} v_j, \tag{6}$$

where v_j represents the j-th text embedding values and $attn_{(q,k_j)}$ denotes the attention score between the patch queries and the j-th text embedding values.

3.3. Multi-Text Patch Alignment for MVS

Patch-level local information contains various detailed cues for FAS [53]. While some CLIP-based methods [18, 20, 36] leverage patch embeddings to capture these details, the lack of patch-level alignment limits the effective utilization of local information.

To address this, we introduce MTPA to ensure effective patch alignment while mitigating the impact of biased text semantics. MTPA applies soft masking to patches with low similarity to the multi-text anchor using soft masking scores within the range (0, 1). These soft-masked patches are processed by an auxiliary classifier, which enhances alignment by providing supervision that increases the similarity between informative patches relevant to spoofing prediction and their corresponding anchors.

Specifically, as shown in Fig. 2, to determine the anchors of the patch alignment, we calculate the mean value of the CLIP text embeddings for the real and spoof classes.

$$\begin{aligned} A_P &= \frac{1}{M}\sum_{j=1}^{M} \mathcal{T}([\mathbf{V}][T_P^j]), \\ A_N &= \frac{1}{M}\sum_{j=1}^{M} \mathcal{T}([\mathbf{V}][T_N^j]), \end{aligned} \tag{7}$$

where $A_P \in \mathbb{R}^D$ and $A_N \in \mathbb{R}^D$ represent the positive and negative anchors, respectively.

Subsequently, the cosine similarity $C \in \mathbb{R}^{B\times L\times 1}$ between the patch embedding $E \in \mathbb{R}^{B\times L\times D}$ and the alignment anchor $A \in \{A_P, A_N\}^B$, which is selected based on the class label of each patch, is calculated as follows:

$$C = E_{norm} \cdot A_{norm}, \tag{8}$$

where $E_{norm} \in \mathbb{R}^{B\times L\times D}$ is the normalized E, and $A_{norm} \in \mathbb{R}^{B\times D\times 1}$ is normalized and expanded A.

Finally, we apply a sigmoid $\sigma(\cdot)$ to the cosine similarity and use the output as soft masking scores $\mathcal{M}$ to suppress patches with lower similarity.

$$\mathcal{M} = \sigma(\alpha C), \tag{9}$$

where α is a scaling factor of the cosine similarity, controlling the range of $\mathcal{M}$. In this paper, we set α to 10 to ensure that $\mathcal{M}$ spans the range (0,1).

These soft-masked patches are aggregated by summation and passed through a fully connected layer FC with softmax $\mathcal{S}$ to obtain the spoofing probability p, which is expressed as in the following:

$$p = \mathcal{S}\left(\text{FC}\left(\sum_{l=1}^{L}(\mathcal{M}\times E_l)\right)\right). \tag{10}$$

Then, cross-entropy (CE) loss with the ground-truth y is computed for MTPA, as formulated in Eq. (11).

$$\mathcal{L}_{\text{MTPA}} = \frac{1}{B}\sum_{k=1}^{B} CE(y_k, p_k). \tag{11}$$

3.4. Total Loss

The total loss of MVP-FAS consists of a classification loss $\mathcal{L}_{\text{cls}}$ and the MTPA loss $\mathcal{L}_{\text{MTPA}}$ for patch alignment. Following prior work [36, 49], we define the classification loss $\mathcal{L}_{\text{cls}}$ as the CE loss between the ground-truth y and the final prediction $\hat{y}$:

$$\mathcal{L}_{\text{cls}} = \frac{1}{B}\sum_{k=1}^{B} CE(y_k, \hat{y}_k). \tag{12}$$

Finally, the total loss is given by the equation below.

$$\mathcal{L}_{\text{total}} = \mathcal{L}_{\text{cls}} + \mathcal{L}_{\text{MTPA}}. \tag{13}$$

4. Experiments

4.1. Experimental Setup

Datasets and Protocols. Following prior works on cross-domain FAS [18, 20, 36, 39, 49], we use two distinct protocols to assess the generalization performance of our proposed MVP-FAS. In Protocol 1, we evaluate our method using four widely recognized FAS benchmark datasets: MSU-MFSD (**M**) [57], CASIA-FASD (**C**) [65], Idiap Replay Attack (**I**) [9], and OULU-NPU (**O**) [5]. In Protocol 2, we use three large-scale FAS benchmark datasets: CASIA-SURF (**S**) [64], CASIA CeFA (**C**) [34], and WMCA (**W**) [16], which include a large number of subjects, extreme domain variations, and extensive samples. Both protocols follow a leave-one-out scheme, which assesses FAS performance on a target dataset based on models trained using the remaining datasets for each protocol.

Evaluation Metrics. For a robust measurement of generalization performance, we employ three widely used FAS metrics: Half Total Error Rate (HTER), Area Under the Curve (AUC), and True Positive Rate (TPR) at a 1% False Positive Rate (FPR) (TPR@FPR=1%).

Method	OCI → M			OMI → C			OCM → I			ICM → O			avg.
	HTER ↓	AUC ↑	TPR@ FPR=1% ↑	HTER ↓	AUC ↑	TPR@ FPR=1% ↑	HTER ↓	AUC ↑	TPR@ FPR=1% ↑	HTER ↓	AUC ↑	TPR@ FPR=1% ↑	HTER ↓
MADDG (CVPR'19) [47]	17.69	88.06	-	24.50	84.51	-	22.19	84.99	-	27.98	80.02	-	23.09
DR-MD-Net (TFIS'20) [54]	17.02	90.10	-	19.68	87.43	-	20.87	86.72	-	25.02	81.47	-	20.64
RFMeta (AAAI'20) [48]	13.89	93.98	-	20.27	88.16	-	17.30	90.48	-	16.45	91.16	-	16.97
NAS-FAS (TPAMI'20) [62]	19.53	89.36	-	16.54	90.11	-	14.51	93.84	-	13.80	93.47	-	16.09
D^2AM (AAAI'21) [8]	12.70	95.66	-	20.98	85.58	-	15.43	91.22	-	15.27	90.87	-	16.09
SDA (AAAI'21) [55]	15.40	91.80	-	24.50	84.40	-	15.60	90.10	-	23.10	84.30	-	19.65
DRDG (IJCAI'21) [38]	12.43	95.13	-	19.05	88.79	-	15.56	91.79	-	15.63	91.75	-	15.66
ANRL (ACM MM'21) [37]	10.83	96.75	-	17.83	89.26	-	16.03	91.04	-	15.67	91.90	-	15.09
SSDG-R (CVPR'20) [24]	7.38	97.17	-	10.44	95.94	-	11.71	96.59	-	15.61	91.54	-	11.28
SSAN-R (CVPR'22) [56]	6.67	98.75	-	10.00	96.67	-	8.88	96.79	-	13.72	96.63	-	9.81
PatchNet (CVPR'22) [53]	7.10	98.46	-	11.33	94.58	-	13.40	95.67	-	11.82	95.07	-	10.91
SA-FAS (CVPR'23) [50]	5.95	96.55	-	8.78	95.37	-	6.58	97.54	-	10.00	96.23	-	7.82
IADG (CVPR'23) [67]	5.41	98.19	-	8.70	96.44	-	10.62	94.50	-	8.86	97.14	-	8.39
CA-MoEiT (IJCV'24) [33]	2.88	98.76	81.43	7.89	97.70	61.33	6.18	98.94	80.00	9.72	96.22	49.44	6.67
GAC-FAS (CVPR'24) [27]	5.00	97.56	-	8.20	95.16	-	4.29	98.87	-	8.60	97.16	-	6.52
CFPL (CVPR'24) [36]	3.09	99.45	94.28	2.56	99.10	66.33	5.43	98.41	85.29	3.33	99.05	90.06	3.60
S-CPTL (ACM MM'24) [18]	1.43	99.17	-	0.89	99.00	-	6.86	98.63	-	4.12	99.02	-	3.33
FGPL (ACM MM'24) [20]	2.86	98.12	-	3.89	98.19	-	3.50	99.54	-	**1.77**	99.23	-	3.01
DiffFAS-V (ECCV'24) [15]	2.86	98.41	-	10.11	96.32	-	6.36	97.89	-	8.11	97.27	-	6.86
BUDoPT (ECCV'24) [39]	**0.95**	99.70	87.12	2.85	98.03	55.00	4.4	98.54	86.46	2.26	98.78	55.25	2.62
MVP-FAS (Ours)	1.71	**99.83**	**98.33**	**0.75**	**99.89**	**99.29**	**1.99**	**99.59**	**95.77**	2.82	**99.49**	**90.85**	**1.82**

Table 1. The results (%) of cross-domain FAS methods on the MSU-MFSD (**M**), CASIA-FASD (**C**), Idiap Replay Attack (**I**), and OULU-NPU (**O**) datasets in Protocol 1. Bold and underlined numbers indicate the best and second-best performances, respectively. The symbols ↑ and ↓ indicate that higher and lower values are preferred, respectively.

Method	CS → W			SW → C			CW → S			avg.
	HTER↓	AUC↑	TPR@FPR=1% ↑	HTER ↓	AUC ↑	TPR@FPR=1% ↑	HTER ↓	AUC ↑	TPR@FPR=1% ↑	HTER ↓
ViT (ECCV'22) [21]	21.04	89.12	30.09	17.12	89.05	22.71	17.16	90.25	30.23	18.44
CLIP-V (ICML'21) [45]	20.00	87.72	16.44	17.67	89.67	20.70	**8.32**	**97.23**	57.28	15.33
CLIP (ICML'21) [45]	17.05	89.37	8.17	15.22	91.99	17.08	9.34	96.62	**60.75**	13.87
CoOp (IJCV'22) [66]	9.52	90.49	10.68	18.30	87.47	11.50	11.37	95.46	40.40	13.06
CFPL (CVPR'24) [36]	9.04	96.48	25.84	14.83	90.36	8.33	8.77	96.83	53.34	10.88
FGPL (ACM MM'24) [20]	14.05	92.65	33.33	19.00	88.53	13.33	11.00	94.72	34.00	14.68
S-CPTL (ACM MM'24) [18]	8.99	94.01	-	12.78	91.64	-	9.48	95.83	-	10.42
MVP-FAS (Ours)	**4.57**	**98.91**	**73.70**	**8.27**	**97.17**	**52.14**	10.19	96.35	60.46	**7.68**

Table 2. The results (%) of cross-domain FAS methods on the CASIA-SURF (**S**), CASIA CeFA (**C**), and WMCA (**W**) datasets in Protocol 2.

Implementation Details. We use a pre-trained CLIP [45] model with ViT-B/16 [12]. For the image encoder, input images are resized to 224×224, resulting in $L = 196$ patch embeddings with a patch size of 16. For the text encoder following CoOp [66], we set the length of the learnable prompt $[\mathbf{V}]$ to 16 and use the same $[\mathbf{V}]$ for all classes. We empirically set the number of positive and negative views to $M = 3$. All feature dimensions in MVP-FAS are set to 512. MVP-FAS is trained for 30 epochs in Protocol 1 and 300 epochs in Protocol 2, both with a batch size of 18. We use the Adam optimizer [25] with a weight decay of 0.001 and initial learning rates of 1e-6 for Protocol 1 and 1e-7 for Protocol 2.

4.2. Cross-domain FAS Performance

Protocol 1. Table 1 shows the results of MVP-FAS and recent SOTA methods for Protocol 1 across the **M**, **C**, **I**, and **O** datasets. MVP-FAS achieves the best average HTER among all methods, including recent CLIP-based models [18, 20, 36, 39]. Notably, MVP-FAS surpasses the previous SOTA method, BUDoPT [39], with a substantial 0.8 percentage points (%p) improvement in average HTER, as well as gains in AUC and TPR@FPR=1%. MVP-FAS also reduces HTER deviations across scenarios to 0.7%, compared to 1.2% for BUDOPT. Moreover, MVP-FAS shows a significant increase in the average TPR@FPR=1%, improving from 83.99% in CFPL [36] to 96.06%.

Protocol 2. We present the results for Protocol 2 in Table 2. Similar to Protocol 1, MVP-FAS achieves the SOTA performance across all metrics on average. MVP-FAS demonstrates a considerable improvement, reducing the average HTER by 2.74%p compared to the previous SOTA method, S-CPTL [18]. Specifically, MVP-FAS significantly reduces HTER by 4.42%p and 4.51%p in the target domains **W** and **C**, respectively, outperforming S-CPTL.

Overall, the experimental results of Protocol 1 and Pro-

Baseline	MVS	MTPA	HTER↓	AUC↑	TPR@FPR=1%↑
✓	-	-	8.59	95.99	60.27
✓	✓	-	7.48	96.87	72.77
✓	-	✓	4.13	99.05	73.09
✓	✓	✓	**1.82**	**99.70**	**96.06**

Table 3. Ablation study on each component of MVP-FAS, with results (%) averaged across all scenarios in Protocol 1.

tocol 2 indicate that MVP-FAS generalizes well to diverse and challenging environments, achieving consistently high performance across all metrics. Moreover, its strong performance in TPR@FPR=1% on cross-domain datasets underscores its reliability in high-security scenarios and its suitability for real-world FR systems.

4.3. Ablation Study

We conduct all ablation studies on the cross-domain scenarios in Protocol 1. To ensure a precise and reliable comparison, all studies except for the single-view text pair comparison (Sec. 4.3.2) are evaluated based on the average scores of HTER(%), AUC(%), and TPR(%)@FPR=1%.

4.3.1. Effectiveness of Each Component

To evaluate the impact of MVS and MTPA components in our MVP-FAS, we establish the baseline model using only the global-aware patch embeddings and our classification head on CLIP. Each component is gradually added to this baseline, and we evaluate their performance. As shown in Table 3, including MVS in the baseline reduces HTER by 1.11%p. This demonstrates that MVS improves the model's generalization ability by capturing multi-view features derived from diverse texts, even if patch embeddings are misaligned. Meanwhile, applying only MTPA leads to a 4.46%p improvement in the baseline HTER. This suggests that patch-level alignment is essential to exploit the local information of patch embeddings in CLIP-based FAS models. Finally, the integration of MTPA and MVS results in significant performance improvements across all metrics, with 6.77%p, 3.71%p, and 35.79%p in terms of HTER, AUC, TPR@FPR=1%, respectively. These results indicate that the combination of multi-view features and aligned patch embeddings synergistically improves generalization.

4.3.2. Prompt Analysis for Multi-View Approach

We use five pairs of positive and negative texts as candidates for the multiple texts in MVP-FAS. The detailed configuration of these pairs is provided in the first column of Table 4. Initially, we evaluate each pair in the single-view setting of the MVS to confirm individual properties, such as domain bias. Table 4 shows the overall average and scenario-specific results on HTER. Among the single-view pairs, 'real face ↔ spoof face' achieves the best average HTER performance of 3.75%. Each text pair performs better in specific domains. For example, although the average performance for 'genuine face ↔ fake face' is relatively low

Single-view(+face)	OCI → M	OMI → C	OCM → I	ICM → O	avg.
(pos↔neg)	HTER(%)↓	HTER(%)↓	HTER(%)↓	HTER(%)↓	HTER(%)↓
real ↔ spoof	4.33	**2.15**	5.11	3.40	**3.75**
bonafide ↔ attack	**2.63**	2.91	5.07	4.43	3.76
genuine ↔ fake	5.00	3.55	**3.84**	**3.31**	3.93
true ↔ false	3.29	2.85	5.71	4.58	4.11
verified ↔ deceptive	5.79	2.56	3.99	4.43	4.19
Ours ($M = 3$)	**1.71**	**0.75**	**1.99**	**2.82**	**1.82**

Table 4. Comparison of HTER among single-view text pairs in Protocol 1. Each text is concisely presented with 'face' omitted.

Number	HTER↓	AUC↑	TPR@FPR=1%↑
$M = 1$	3.75	99.09	86.94
$M = 2$	2.89 (-0.86)	99.47 (+0.38)	91.75 (+4.81)
$M = 3$	**1.82 (-1.93)**	**99.70 (+0.61)**	**96.06 (+9.12)**
$M = 4$	1.95 (-1.80)	99.66 (+0.57)	93.87 (+6.93)
$M = 5$	1.97 (-1.78)	99.63 (+0.54)	92.84 (+5.90)

Table 5. Ablation study on the number of multi-views, with each result (%) indicating the average across all scenarios in Protocol 1.

with 3.93%, it individually achieves the best score of 3.84% for **OCM→I**. Similarly, the 'bonafide face ↔ attack face' achieves the highest score of 2.63% for **OCI→M**. However, in terms of generalization, using only one text pair may hinder the model's capability for cross-domain FAS.

4.3.3. Effectiveness of Multi-View Number

To investigate the optimal number of multi-views, we construct models that progressively incorporate each text pair in the order of higher single-view HTER (Sec. 4.3.2). As shown in Table 5, all multi-view settings outperform the single-view setting ($M = 1$). Notably, multi-view performance improves even when incorporating a text pair that initially exhibits lower performance in the single-view setting. These experimental results indicate that the multi-view setting enhances generalization ability for cross-domain FAS. The best overall performance is observed at $M = 3$. However, it slightly declines as more text pairs are added ($M \geq 4$), likely due to increased noise. Nevertheless, the multi-view settings consistently surpass the single-view settings.

4.3.4. Types of MTPA Anchor

To determine the optimal anchor value for patch alignment across multiple texts, we compare three methods: a single text pair 'real ↔ spoof', which shows the best performance in Table 4 as the anchor (Single), aligning all multi-text individually as anchors (Individual), and utilizing the mean value of the multi-text as the anchor (Mean). As shown in Table 6, the Individual approach performs worse than using a single text, although it uses the same number of multi-texts. These results suggest that treating each text individually as an anchor causes them to act as outliers in the text embedding space, leading to lower performance. Using the mean value of multi-texts as an anchor, MTPA reduces the influence of these outliers, achieving a more generalized text representation compared to using a single text, thereby

resulting in superior performance.

Type	HTER↓	AUC↑	TPR@FPR=1%↑
Single	3.98	99.15	75.84
Individual	4.58	98.69	60.00
Mean (Ours)	**1.82**	**99.70**	**96.06**

Table 6. Ablation study on the anchor of MTPA, with each result (%) representing the average performance in Protocol 1.

4.3.5. Effectiveness of Slot Attention in MVS

As shown in Table 7, we perform an ablation study to evaluate the effectiveness of slot attention in MVS, comparing it against two alternative methods that also incorporate text and patch information. The first variant uses a similarity-based approach, predicting outcomes by calculating the cosine similarity between the mean of global-aware patch embeddings and text embeddings, similar to CLIP. The second variant employs cross-attention, with texts as queries and patches as keys and values. Even though they utilize the same global-aware patch embedding, slot attention surpasses other methods across all metrics. This suggests that slot attention effectively captures global-local patch information through multi-view representation.

Method	HTER↓	AUC↑	TPR@FPR=1%↑
Similarity	5.26	98.50	76.37
Cross-attention	5.68	98.31	74.97
MVS (Ours)	**1.82**	**99.70**	**96.06**

Table 7. Ablation study to evaluate the impact of MVS, with each result (%) indicating the average across all scenarios in Protocol 1.

4.3.6. Impact of Global-Aware Patch Embedding

Table 8 presents a performance comparison between global-aware patch embedding and original patch embedding in MVS. We observe that global-aware patch embedding outperforms regular patch embedding, suggesting that incorporating a CLS token to provide global context effectively improves overall performance. We believe that global-aware patch embedding enables a more effective allocation of text embeddings in CLIP-based MVP-FAS, because the original CLIP is pre-trained to align the CLS token with text.

	HTER↓	AUC↑	TPR@FPR=1%↑
Patch embedding	5.39	97.92	75.78
GAPE	**1.82**	**99.70**	**96.06**

Table 8. Ablation study on global-aware patch embedding (GAPE), with each result (%) representing the average across all scenarios in Protocol 1.

4.4. Visualization of Multi-Views

We visualize multi-view attention scores from MVS, providing more informative insights into predictions than the existing visualization method [6] used in prior works [20, 36, 49]. As shown in Fig. 4, MVS's multi-view visualization illustrates the degree to which positive and negative texts are assigned across all patches, indicating the model's

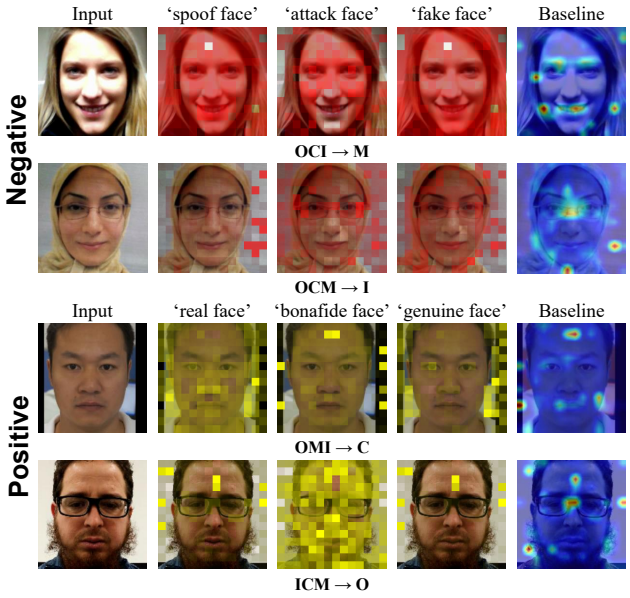

Figure 4. **Visualization results for each view on real and spoof images across all sub-protocols in Protocol 1.** We visualize multi-view attention scores in the first stage of MVS. Baseline (Sec. 4.3.1) indicates the attention map [6], following the visualization method used in previous studies [20, 36, 49]. For better visibility, we visualize positive scores in yellow and negative scores in red.

basis for determining spoofing or real. In negative samples (**OCI** $\rightarrow$ **M** and **OCM** $\rightarrow$ **I**), the assigned texts primarily focus on the eye and mouth regions, some background areas, and facial edges that reveal depth differences. For positive samples (**OMI** $\rightarrow$ **C** and **ICM** $\rightarrow$ **O**), MVS tends to focus on the overall texture or style of the image, as well as light reflections on features like the nose and forehead when identifying a real face. By providing diverse positive and negative views, our multi-view visualization suggests a way to overcome the limitations of the existing attention map [6], which lacks clarity in explaining the relevance of activated features.

5. Conclusion

We propose MVP-FAS, a novel framework that includes MVS and MTPA, both of which leverage paraphrased multi-text to enhance cross-domain generalization. To the best of our knowledge, MVP-FAS is the first VLM-based FAS method to incorporate slot attention. Our MVP-FAS markedly outperforms existing VLM-based FAS methods across cross-domain datasets, achieving SOTA performance and providing interpretable visualizations. These results demonstrate that capturing diverse fine-grained information and global context via MVS, while aligning patches through MTPA can significantly improve the model's generalization ability in FAS. We believe that our method will benefit other computer vision tasks that require fine-grained recognition.

6. Acknowledgment

This work was supported by the National Research Foundation of Korea (NRF) grant funded by the Korea government (MSIT) (No. 2023R1A2C200337911 and No. RS-2023-00220762) and the Institute of Information & Communications Technology Planning & Evaluation (IITP) grant funded by the Korea government (MSIT) (No.RS-2025-02303870, Software Technology for Efficient Multimodal Visual Information Processing in High-Speed Spatial Interactions) and (No.RS-2024-00439762, Developing Techniques for Analyzing and Assessing Vulnerabilities, and Tools for Confidentiality Evaluation in Generative AI Models).

References

[1] Josh Achiam, Steven Adler, Sandhini Agarwal, Lama Ahmad, Ilge Akkaya, Florencia Leoni Aleman, Diogo Almeida, Janko Altenschmidt, Sam Altman, Shyamal Anadkat, et al. Gpt-4 technical report. *arXiv preprint arXiv:2303.08774*, 2023. 3

[2] Ioana Bica, Anastasija Ili'c, Matthias Bauer, Goker Erdogan, Matko Bovsnjak, Christos Kaplanis, Alexey A. Gritsenko, Matthias Minderer, Charles Blundell, Razvan Pascanu, and Jovana Mitrovi'c. Improving fine-grained understanding in image-text pre-training. *ArXiv*, abs/2401.09865, 2024. 3

[3] Zinelabidine Boulkenafet, Jukka Komulainen, and Abdenour Hadid. Face anti-spoofing based on color texture analysis. In *2015 IEEE international conference on image processing (ICIP)*, pages 2636–2640. IEEE, 2015. 1, 2

[4] Zinelabidine Boulkenafet, Jukka Komulainen, and Abdenour Hadid. Face antispoofing using speeded-up robust features and fisher vector encoding. *IEEE Signal Processing Letters*, 24(2):141–145, 2016. 1, 2

[5] Zinelabinde Boulkenafet, Jukka Komulainen, Lei Li, Xiaoyi Feng, and Abdenour Hadid. Oulu-npu: A mobile face presentation attack database with real-world variations. In *2017 12th IEEE international conference on automatic face & gesture recognition (FG 2017)*, pages 612–618. IEEE, 2017. 2, 5

[6] Hila Chefer, Shir Gur, and Lior Wolf. Generic attention-model explainability for interpreting bi-modal and encoder-decoder transformers. In *Proceedings of the IEEE/CVF International Conference on Computer Vision*, pages 397–406, 2021. 8

[7] Shunxin Chen, Ajian Liu, Junze Zheng, Jun Wan, Kailai Peng, Sergio Escalera, and Zhen Lei. Mixture-of-attack-experts with class regularization for unified physical-digital face attack detection. In *Proceedings of the AAAI Conference on Artificial Intelligence*, pages 2195–2203, 2025. 1

[8] Zhihong Chen, Taiping Yao, Kekai Sheng, Shouhong Ding, Ying Tai, Jilin Li, Feiyue Huang, and Xinyu Jin. Generalizable representation learning for mixture domain face anti-spoofing. In *Proceedings of the AAAI conference on artificial intelligence*, pages 1132–1139, 2021. 6

[9] Ivana Chingovska, André Anjos, and Sébastien Marcel. On the effectiveness of local binary patterns in face anti-spoofing. In *2012 BIOSIG-proceedings of the international conference of biometrics special interest group (BIOSIG)*, pages 1–7. IEEE, 2012. 1, 2, 5

[10] Kyunghyun Cho, Bart Van Merriënboer, Caglar Gulcehre, Dzmitry Bahdanau, Fethi Bougares, Holger Schwenk, and Yoshua Bengio. Learning phrase representations using rnn encoder-decoder for statistical machine translation. pages 1724–1734, 2014. 4

[11] Tiago de Freitas Pereira, André Anjos, José Mario De Martino, and Sébastien Marcel. Lbp- top based countermeasure against face spoofing attacks. In *Computer Vision-ACCV 2012 Workshops: ACCV 2012 International Workshops, Daejeon, Korea, November 5-6, 2012, Revised Selected Papers, Part I 11*, pages 121–132. Springer, 2013. 1, 2

[12] Alexey Dosovitskiy, Lucas Beyer, Alexander Kolesnikov, Dirk Weissenborn, Xiaohua Zhai, Thomas Unterthiner, Mostafa Dehghani, Matthias Minderer, Georg Heigold, Sylvain Gelly, et al. An image is worth 16x16 words: Transformers for image recognition at scale. In *International Conference on Learning Representations*, 2020. 6

[13] Ke Fan, Zechen Bai, Tianjun Xiao, Dominik Zietlow, Max Horn, Zixu Zhao, Carl-Johann Simon-Gabriel, Mike Zheng Shou, Francesco Locatello, Bernt Schiele, et al. Unsupervised open-vocabulary object localization in videos. In *Proceedings of the IEEE/CVF International Conference on Computer Vision*, pages 13747–13755, 2023. 3

[14] Hao Fang, Ajian Liu, Haocheng Yuan, Junze Zheng, Dingheng Zeng, Yanhong Liu, Jiankang Deng, Sergio Escalera, Xiaoming Liu, Jun Wan, et al. Unified physical-digital face attack detection. *arXiv preprint arXiv:2401.17699*, 2024. 1

[15] Xinxu Ge, Xin Liu, Zitong Yu, Jingang Shi, Chun Qi, Jie Li, and Heikki Kälviäinen. Difffas: Face anti-spoofing via generative diffusion models. In *European Conference on Computer Vision*, 2024. 6

[16] Anjith George, Zohreh Mostaani, David Geissenbuhler, Olegs Nikisins, André Anjos, and Sébastien Marcel. Biometric face presentation attack detection with multi-channel convolutional neural network. *IEEE transactions on information forensics and security*, 15:42–55, 2019. 2, 5

[17] Andy Greenberg. Hackers say they've broken face id a week after iphone x release. *Wired, November*, 12, 2017. 1

[18] Jiabao Guo, Huan Liu, Yizhi Luo, Xueli Hu, Hang Zou, Yuan Zhang, Hui Liu, and Bo Zhao. Style-conditional prompt token learning for generalizable face anti-spoofing. In *ACM Multimedia*, 2024. 1, 2, 4, 5, 6

[19] Chengyang Hu, Ke-Yue Zhang, Taiping Yao, Shouhong Ding, and Lizhuang Ma. Rethinking generalizable face anti-spoofing via hierarchical prototype-guided distribution refinement in hyperbolic space. In *Proceedings of the IEEE/CVF Conference on Computer Vision and Pattern Recognition*, pages 1032–1041, 2024. 1

[20] Xueli Hu, Huan Liu, Haocheng Yuan, Zhiyang Fu, Yizhi Luo, Ning Zhang, Hang Zou, Gan Jianwen, and Yuan Zhang. Fine-grained prompt learning for face anti-spoofing. In *ACM Multimedia*, 2024. 1, 2, 5, 6, 8

[21] Hsin-Ping Huang, Deqing Sun, Yaojie Liu, Wen-Sheng Chu, Taihong Xiao, Jinwei Yuan, Hartwig Adam, and Ming-Hsuan Yang. Adaptive transformers for robust few-shot cross-domain face anti-spoofing. In *European conference on computer vision*, pages 37–54. Springer, 2022. 6

[22] Pei-Kai Huang, Cheng-Hsuan Chiang, Tzu-Hsien Chen, Jun-Xiong Chong, Tyng-Luh Liu, and Chiou-Ting Hsu. One-class face anti-spoofing via spoof cue map-guided feature learning. In *Proceedings of the IEEE/CVF Conference on Computer Vision and Pattern Recognition*, pages 277–286, 2024. 1

[23] Jingyang Huo, Qiang Sun, Boyan Jiang, Haitao Lin, and Yanwei Fu. Geovln: Learning geometry-enhanced visual representation with slot attention for vision-and-language navigation. In *Proceedings of the IEEE/CVF Conference on Computer Vision and Pattern Recognition*, pages 23212–23221, 2023. 3

[24] Yunpei Jia, Jie Zhang, Shiguang Shan, and Xilin Chen. Single-side domain generalization for face anti-spoofing. In *Proceedings of the IEEE/CVF Conference on Computer Vision and Pattern Recognition*, pages 8484–8493, 2020. 1, 6

[25] Diederik P Kingma. Adam: A method for stochastic optimization. *arXiv preprint arXiv:1412.6980*, 2014. 6

[26] Jukka Komulainen, Abdenour Hadid, and Matti Pietikäinen. Context based face anti-spoofing. In *2013 IEEE sixth international conference on biometrics: theory, applications and systems (BTAS)*, pages 1–8. IEEE, 2013. 1, 2

[27] Binh M Le and Simon S Woo. Gradient alignment for cross-domain face anti-spoofing. In *Proceedings of the IEEE/CVF Conference on Computer Vision and Pattern Recognition*, pages 188–199, 2024. 1, 2, 6

[28] Haoliang Li, Wen Li, Hong Cao, Shiqi Wang, Feiyue Huang, and Alex C Kot. Unsupervised domain adaptation for face anti-spoofing. *IEEE Transactions on Information Forensics and Security*, 13(7):1794–1809, 2018. 2

[29] Lei Li, Xiaoyi Feng, Zinelabidine Boulkenafet, Zhaoqiang Xia, Mingming Li, and Abdenour Hadid. An original face anti-spoofing approach using partial convolutional neural network. In *2016 sixth international conference on image processing theory, tools and applications (IPTA)*, pages 1–6. IEEE, 2016. 1, 2

[30] Xiaobai Li, Jukka Komulainen, Guoying Zhao, Pong-Chi Yuen, and Matti Pietikäinen. Generalized face anti-spoofing by detecting pulse from face videos. In *2016 23rd International Conference on Pattern Recognition (ICPR)*, pages 4244–4249. IEEE, 2016. 1, 2

[31] Yongze Li, Ning Li, Ajian Liu, Hui Ma, Liying Yang, Xihong Chen, Zhiyao Liang, Yanyan Liang, Jun Wan, and Zhen Lei. Fa^{3}-clip: Frequency-aware cues fusion and attack-agnostic prompt learning for unified face attack detection. *arXiv preprint arXiv:2504.00454*, 2025. 1

[32] Xun Lin, Shuai Wang, Rizhao Cai, Yizhong Liu, Ying Fu, Wenzhong Tang, Zitong Yu, and Alex Kot. Suppress and rebalance: Towards generalized multi-modal face anti-spoofing. In *Proceedings of the IEEE/CVF Conference on Computer Vision and Pattern Recognition*, pages 211–221, 2024. 1

[33] Ajian Liu. Ca-moeit: Generalizable face anti-spoofing via dual cross-attention and semi-fixed mixture-of-expert. *International Journal of Computer Vision*, 132(11):5439–5452, 2024. 6

[34] Ajian Liu, Zichang Tan, Jun Wan, Sergio Escalera, Guodong Guo, and Stan Z Li. Casia-surf cefa: A benchmark for multi-modal cross-ethnicity face anti-spoofing. In *Proceedings of the IEEE/CVF winter conference on applications of computer vision*, pages 1179–1187, 2021. 2, 5

[35] Ajian Liu, Hui Ma, Junze Zheng, Haocheng Yuan, Xiaoyuan Yu, Yanyan Liang, Sergio Escalera, Jun Wan, and Zhen Lei. Fm-clip: Flexible modal clip for face anti-spoofing. In *Proceedings of the 32nd ACM International Conference on Multimedia*, pages 8228–8237, 2024. 3

[36] Ajian Liu, Shuai Xue, Jianwen Gan, Jun Wan, Yanyan Liang, Jiankang Deng, Sergio Escalera, and Zhen Lei. Cfpl-fas: Class free prompt learning for generalizable face anti-spoofing. In *Proceedings of the IEEE/CVF Conference on Computer Vision and Pattern Recognition*, pages 222–232, 2024. 1, 2, 4, 5, 6, 8

[37] Shubao Liu, Ke-Yue Zhang, Taiping Yao, Mingwei Bi, Shouhong Ding, Jilin Li, Feiyue Huang, and Lizhuang Ma. Adaptive normalized representation learning for generalizable face anti-spoofing. In *Proceedings of the 29th ACM international conference on multimedia*, pages 1469–1477, 2021. 2, 6

[38] Shubao Liu, Ke-Yue Zhang, Taiping Yao, Kekai Sheng, Shouhong Ding, Ying Tai, Jilin Li, Yuan Xie, and Lizhuang Ma. Dual reweighting domain generalization for face presentation attack detection. *arXiv preprint arXiv:2106.16128*, 2021. 2, 6

[39] Si-Qi Liu, Qirui Wang, and Pong C Yuen. Bottom-up domain prompt tuning for generalized face anti-spoofing. In *European Conference on Computer Vision*, 2024. 1, 2, 5, 6

[40] Yuchen Liu, Yabo Chen, Wenrui Dai, Mengran Gou, Chun-Ting Huang, and Hongkai Xiong. Source-free domain adaptation with contrastive domain alignment and self-supervised exploration for face anti-spoofing. In *European Conference on Computer Vision*, pages 511–528. Springer, 2022. 2

[41] Francesco Locatello, Dirk Weissenborn, Thomas Unterthiner, Aravindh Mahendran, Georg Heigold, Jakob Uszkoreit, Alexey Dosovitskiy, and Thomas Kipf. Object-centric learning with slot attention. *Advances in neural information processing systems*, 33:11525–11538, 2020. 2, 4

[42] Jishnu Mukhoti, Tsung-Yu Lin, Omid Poursaeed, Rui Wang, Ashish Shah, Philip HS Torr, and Ser-Nam Lim. Open vocabulary semantic segmentation with patch aligned contrastive learning. In *Proceedings of the IEEE/CVF Conference on Computer Vision and Pattern Recognition*, pages 19413–19423, 2023. 2, 3

[43] Gang Pan, Lin Sun, Zhaohui Wu, and Shihong Lao. Eyeblink-based anti-spoofing in face recognition from a generic webcamera. In *2007 IEEE 11th international conference on computer vision*, pages 1–8. IEEE, 2007. 2

[44] Keyurkumar Patel, Hu Han, and Anil K Jain. Secure face unlock: Spoof detection on smartphones. *IEEE transactions on information forensics and security*, 11(10):2268–2283, 2016. 1, 2

[45] Alec Radford, Jong Wook Kim, Chris Hallacy, Aditya Ramesh, Gabriel Goh, Sandhini Agarwal, Girish Sastry, Amanda Askell, Pamela Mishkin, Jack Clark, et al. Learning transferable visual models from natural language supervision. In *International conference on machine learning*, pages 8748–8763. PMLR, 2021. 1, 2, 3, 6

[46] Mehdi SM Sajjadi, Daniel Duckworth, Aravindh Mahendran, Sjoerd Van Steenkiste, Filip Pavetic, Mario Lucic, Leonidas J Guibas, Klaus Greff, and Thomas Kipf. Object scene representation transformer. *Advances in neural information processing systems*, 35:9512–9524, 2022. 3

[47] Rui Shao, Xiangyuan Lan, Jiawei Li, and Pong C Yuen. Multi-adversarial discriminative deep domain generalization for face presentation attack detection. In *Proceedings of the IEEE/CVF conference on computer vision and pattern recognition*, pages 10023–10031, 2019. 1, 6

[48] Rui Shao, Xiangyuan Lan, and Pong C Yuen. Regularized fine-grained meta face anti-spoofing. In *Proceedings of the AAAI conference on artificial intelligence*, pages 11974–11981, 2020. 6

[49] Koushik Srivatsan, Muzammal Naseer, and Karthik Nandakumar. Flip: Cross-domain face anti-spoofing with language guidance. In *Proceedings of the IEEE/CVF International Conference on Computer Vision*, pages 19685–19696, 2023. 1, 2, 5, 8

[50] Yiyou Sun, Yaojie Liu, Xiaoming Liu, Yixuan Li, and Wen-Sheng Chu. Rethinking domain generalization for face anti-spoofing: Separability and alignment. In *Proceedings of the IEEE/CVF conference on computer vision and pattern recognition*, pages 24563–24574, 2023. 2, 6

[51] Hao Tan, Jun Li, Yizhuang Zhou, Jun Wan, Zhen Lei, and Xiangyu Zhang. Compound text-guided prompt tuning via image-adaptive cues. In *Proceedings of the AAAI Conference on Artificial Intelligence*, pages 5061–5069, 2024. 2

[52] Vidit Vidit, Martin Engilberge, and Mathieu Salzmann. Clip the gap: A single domain generalization approach for object detection. In *Proceedings of the IEEE/CVF conference on computer vision and pattern recognition*, pages 3219–3229, 2023. 2

[53] Chien-Yi Wang, Yu-Ding Lu, Shang-Ta Yang, and Shang-Hong Lai. Patchnet: A simple face anti-spoofing framework via fine-grained patch recognition. In *Proceedings of the IEEE/CVF Conference on Computer Vision and Pattern Recognition*, pages 20281–20290, 2022. 5, 6

[54] Guoqing Wang, Hu Han, Shiguang Shan, and Xilin Chen. Unsupervised adversarial domain adaptation for cross-domain face presentation attack detection. *IEEE Transactions on Information Forensics and Security*, 16:56–69, 2020. 1, 6

[55] Jingjing Wang, Jingyi Zhang, Ying Bian, Youyi Cai, Chunmao Wang, and Shiliang Pu. Self-domain adaptation for face anti-spoofing. In *Proceedings of the AAAI conference on artificial intelligence*, pages 2746–2754, 2021. 6

[56] Zhuo Wang, Zezheng Wang, Zitong Yu, Weihong Deng, Jiahong Li, Tingting Gao, and Zhongyuan Wang. Domain generalization via shuffled style assembly for face anti-spoofing. In *Proceedings of the IEEE/CVF conference on computer vision and pattern recognition*, pages 4123–4133, 2022. 2, 6

[57] Di Wen, Hu Han, and Anil K Jain. Face spoof detection with image distortion analysis. *IEEE Transactions on Information Forensics and Security*, 10(4):746–761, 2015. 2, 5

[58] Jilan Xu, Junlin Hou, Yuejie Zhang, Rui Feng, Yi Wang, Yu Qiao, and Weidi Xie. Learning open-vocabulary semantic segmentation models from natural language supervision. In *Proceedings of the IEEE/CVF conference on computer vision and pattern recognition*, pages 2935–2944, 2023. 3

[59] Jiaqi Xu, Cuiling Lan, Wenxuan Xie, Xuejin Chen, and Yan Lu. Slot-vlm: Object-event slots for video-language modeling. *Advances in Neural Information Processing Systems*, 37:632–659, 2025. 3

[60] Charig Yang, Hala Lamdouar, Erika Lu, Andrew Zisserman, and Weidi Xie. Self-supervised video object segmentation by motion grouping. In *Proceedings of the IEEE/CVF International Conference on Computer Vision*, pages 7177–7188, 2021. 3

[61] Jianwei Yang, Zhen Lei, Shengcai Liao, and Stan Z Li. Face liveness detection with component dependent descriptor. In *2013 International Conference on Biometrics (ICB)*, pages 1–6. IEEE, 2013. 1, 2

[62] Zitong Yu, Jun Wan, Yunxiao Qin, Xiaobai Li, Stan Z Li, and Guoying Zhao. Nas-fas: Static-dynamic central difference network search for face anti-spoofing. *IEEE transactions on pattern analysis and machine intelligence*, 43(9):3005–3023, 2020. 6

[63] Zitong Yu, Chenxu Zhao, Zezheng Wang, Yunxiao Qin, Zhuo Su, Xiaobai Li, Feng Zhou, and Guoying Zhao. Searching central difference convolutional networks for face anti-spoofing. In *Proceedings of the IEEE/CVF conference on computer vision and pattern recognition*, pages 5295–5305, 2020. 2

[64] Shifeng Zhang, Ajian Liu, Jun Wan, Yanyan Liang, Guodong Guo, Sergio Escalera, Hugo Jair Escalante, and Stan Z Li. Casia-surf: A large-scale multi-modal benchmark for face anti-spoofing. *IEEE Transactions on Biometrics, Behavior, and Identity Science*, 2(2):182–193, 2020. 2, 5

[65] Zhiwei Zhang, Junjie Yan, Sifei Liu, Zhen Lei, Dong Yi, and Stan Z Li. A face antispoofing database with diverse attacks. In *2012 5th IAPR international conference on Biometrics (ICB)*, pages 26–31. IEEE, 2012. 1, 2, 5

[66] Kaiyang Zhou, Jingkang Yang, Chen Change Loy, and Ziwei Liu. Learning to prompt for vision-language models. *International Journal of Computer Vision*, 130(9):2337–2348, 2022. 3, 6

[67] Qianyu Zhou, Ke-Yue Zhang, Taiping Yao, Xuequan Lu, Ran Yi, Shouhong Ding, and Lizhuang Ma. Instance-aware domain generalization for face anti-spoofing. In *Proceedings of the IEEE/CVF Conference on Computer Vision and Pattern Recognition*, pages 20453–20463, 2023. 2, 6

[68] Qianyu Zhou, Ke-Yue Zhang, Taiping Yao, Xuequan Lu, Shouhong Ding, and Lizhuang Ma. Test-time domain generalization for face anti-spoofing. In *Proceedings of the IEEE/CVF Conference on Computer Vision and Pattern Recognition*, pages 175–187, 2024. 1

[69] Ziqin Zhou, Yinjie Lei, Bowen Zhang, Lingqiao Liu, and Yifan Liu. Zegclip: Towards adapting clip for zero-shot se-

mantic segmentation. In *Proceedings of the IEEE/CVF Conference on Computer Vision and Pattern Recognition*, pages 11175–11185, 2023. 2